# Zircon (U-Th)/He Closure Temperature Lower Than Apatite Thermochronometric Systems: Reconciliation of a Paradox

Benjamin Gérard, Xavier Robert, Cécile Gautheron, Djordje Grujic, Laurence Audin, Matthias Bernet, Mélanie Balvay

*Article*

# Zircon (U-Th)/He closure temperature lower than apatite thermochronometric systems: reconciliation of a paradox

**Benjamin Gérard [1,*], Xavier Robert [1], Cécile Gautheron [2], Djordje Grujic [3], Laurence Audin [1], Matthias Bernet [1] and Mélanie Balvay [1]**

[1] Université Grenoble Alpes, Université Savoie Mont Blanc, CNRS, IRD, IFSTTAR, ISTerre, 38000 Grenoble, France
[2] Université Paris-Saclay, CNRS, GEOPS, 91405, Orsay, France
[3] Dalhousie University, Halifax, Canada
* Correspondence: benjamin.gerard.alpes@gmail.com; Presently at GET, Université de Toulouse, CNRS, IRD, UPS, Toulouse, France

**Abstract:** We present here seven new zircon (U-Th)/He (ZHe) ages and three new zircon fission track ages (ZFT) analyzed from an age-elevation profile (Machu Picchu, Peru). ZFT data present older ages in comparison with the other thermochronological data, whereas the ZHe data interestingly present similar ages than the ones obtained with apatite (U-Th)/He (AHe). It has been proposed that He retention in zircon is linked to the damage dose, with an evolution of the closure-temperature from low values associated to low $\alpha$-dose (<$10^{16}$ $\alpha$/g), subsequently increasing before decreasing again at very high $\alpha$-dose (>$10^{18}$ $\alpha$ /g). Studies have been focused on the He diffusion behavior at high $\alpha$-dose, but little is known at low dose. We propose that the ZHe closure temperature at $\alpha$-dose ranging from $0.6\times10^{15}$ to $4\times10^{16}$ $\alpha$/g is in the range of ~60-80°C. This value is lower than the one proposed in the current damage model ZRDAAM and demonstrates that the ZHe and AHe methods could have similar closure temperatures at low $\alpha$-dose (*i.e.* similar ages). These new data strengthen our previous geological conclusions and even highlight an about twice more important cooling rate than the one deduced from AHe and apatite fission-track data alone registered at Machu Picchu.

**Keywords:** Zircon thermochronometry; $\alpha$-dose; (U-Th)/He; Andes, Machu Picchu.

## 1. Introduction

To quantitatively unravel tectonics and/or relief evolution of a given region, low-temperature thermochronology methods such as (U-Th)/He and fission track dating of apatite (AHe and AFT, respectively) or zircon (ZHe and ZFT, respectively), are often used together [*e.g.* 1,2]. The ZFT and ZHe methods are generally known to record higher temperatures or deeper processes than the AFT and AHe methods [3,4] because of their higher closure temperatures [*e.g.* 5–7]. Also, for a given mineral, (U-Th)/He thermochronometry is generally considered more sensitive to lower temperatures than fission track thermochronology [1,5]. Today, these techniques are routinely applied, and numerous studies are published each year for exhumation quantification purposes. But, for over a decade, methodological studies highlighted that He diffusion in apatites and zircons are strongly dependent on the radiation damage dose increasing the range of the closure temperature, as important age dispersion with positive AHe-age, and positive and negative ZHe-ages correlations are now often observed [*e.g.* 8,9 for zircons], [*e.g.* 10–13 for apatites].

For the ZHe method, He diffusion behavior in zircon is still debated. Based on age-effective Uranium concentration (eU) correlations, [14,15] proposed that radiation damages produced during U and Th decay influence the He retention and loss in zircons, and proposed the algorithm ZRDAAM to model the damage production, annealing and He diffusion in the damaged zircon similar to RDAAM for apatite [12]. In this model, damages firstly trap He until a threshold where damages coalesce, leading to damages

connectivity and the creation of fast He diffusion pathways [14]. In addition, several studies discuss about the damage model parameters such as the threshold value [*e.g.* 16,17] or failed to numerically reproduce high-damaged zircons with this classic He kinetic model as the minerals appear more He retentive than predicted [9].

On the other hand, [17] proposed a trapping model and also a non-linear relationship between the closure temperature and the $\alpha$-damage increase, illustrating the importance of $\alpha$-dose for the closure temperature. The $\alpha$-dose corresponds to the total radiation damage that accumulated in the crystal lattice, mostly due to $\alpha$ recoil. It depends on both eU and since when the mineral began to accumulate damages. This model explains not only zircon data presenting age-eU and age-diffusion domain (ESR) correlation, but also data with no such correlation. In the range of geologically possible $\alpha$-dose, this model predicts closure temperatures consistent with settings within middle to high range of $\alpha$-dose ($10^{17}$ – $5\times10^{18}$ $\alpha$/g), but there do not exist enough available data in low $\alpha$-dose settings to confirm the model at any existing $\alpha$-dose. [17] only suggest indirectly, a closure temperature for a low $\alpha$-dose range ($<1\times10^{15}$ $\alpha$/g) of 60-100°C with the volcanic zircon data of [18].

In this article, we propose to provide new data with low $\alpha$-dose to fill this current gap and improve this model with direct observations. Based on new ZHe, ZFT and published AHe and AFT data from the Machu Picchu (Peru) vertical profile [19] (Figure 1), we show that in case of low $\alpha$-dose, ZHe closure temperatures are closer to AHe closure temperatures than previously proposed, and thus present younger ages than AFT and sometimes even younger than AHe, as predicted by the [17] model. This article does not specifically focus on the geological interpretation of these data, but will somewhat discuss the implications of our results for the geological evolution of the region where samples were collected.

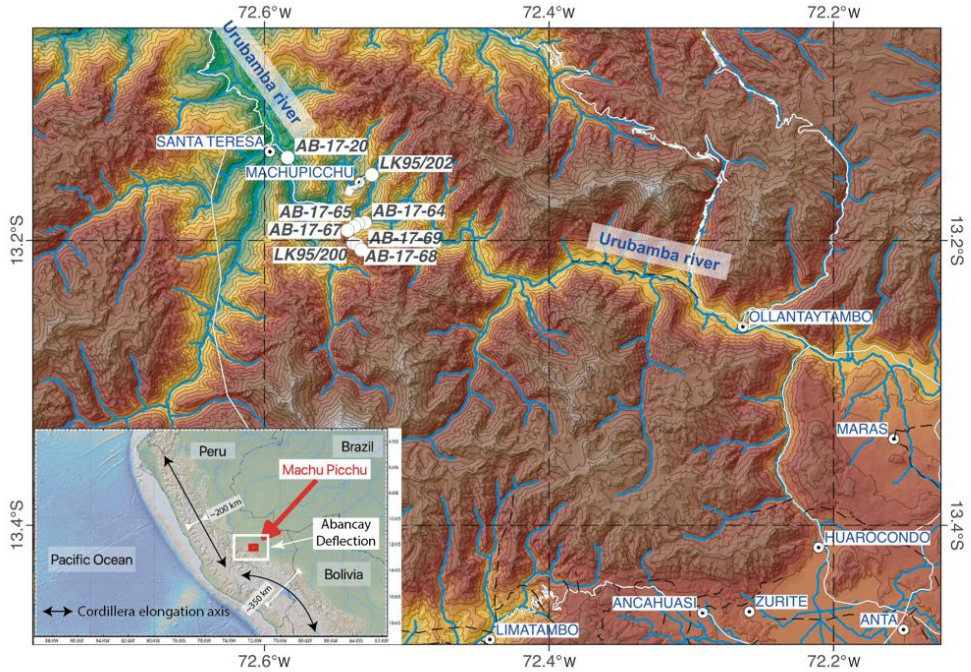


**Figure 1.** Location of the thermochronologic data (white dots) closed to the Machu Picchu archeological site in the Urubamba valley (Peru). The inset shows the location of the main map in Peru.

## 2. Geological settings

The Machu Picchu age-elevation profile is located at the center of an Andean morpho-tectonic peculiarity: The Abancay Deflection [20]. The Abancay Deflection tectonically delimits the Bolivian Orocline to the south (Eocene–Early Miocene rotation of up to ~65°) and the straight and narrow Andes to the north in Peru [Figure 1; 20,21]. It partly lies in the Eastern Cordillera (northern part of the Abancay Deflection) where numerous

Permo-Triassic batholiths emplaced into Paleozoic metasedimentary rocks of the Marañon complex [22]. Among them, the granitic Machu Picchu Batholith we sampled (Figure 1) emplaced at 222 ± 7 Ma in the core of the Abancay Deflection [23]. The Eastern Cordillera shows high elevation and relief. [24] proposed it has been a long-lived structural high because of absence of a Meso-Cenozoic sedimentary cover. Young AFT and AHe ages obtained along a quasi-vertical transect of the Machu Picchu Batholith, however, evidence unexpected rapid and recent exhumation at a rate of 1.2 km/Myr, initiated at ~5 Ma [25,26]. This exhumation phase is also evidenced in another vertical profile 30 km further east in the Ocobamba valley, still in the core of the Abancay Deflection [26]. In the southern part of the Abancay Deflection, the Altiplano domain is tectonically decoupled from the Eastern Cordillera along the regional crustal-scale Apurimac fault system [Figure 1; 26,27]. In the Altiplano, Eocene plutons [50-30 Ma; 28] emplaced into Meso-Cenozoic sediments [29]. As opposed to the core of the Abancay Deflection (Eastern Cordillera), the Altiplano did not experience recent exhumation acceleration, but rather slow and constant exhumation (~0.2 km/Myr) since 40 Ma [26,30]. Because of the differential exhumation pattern, with higher exhumation rates identified at the core of the Abancay Deflection, the active tectonics and curved fault patterns, it has been proposed that the Abancay Deflection should be a tectonic syntaxis comparable to the ones described in the Himalaya for instance [26].

## 3. Materials and Methods

We collected seven samples along a 1.9-km-quasi-vertical profile in the Machu Picchu batholith. We performed ZHe and ZFT dating from the same samples presented in [19]. On the field, we collected the freshest in-situ rocks avoiding to sample nearby traces of fluid circulation. The samples were crushed and sieved to extract the 100-160 μm fractions in the Géode laboratory (Lyon, France). Zircon crystals were consequently concentrated using standard magnetic and heavy-liquid separation techniques at the GTC laboratory (ISTerre, Grenoble, France).

Zircons were processed at the Dalhousie Noble Gas Extraction Laboratory (Halifax, Canada) for (U-Th)/He dating. They were analyzed following the methods described in [4,5,31]. In parallel, 2 Fish Canyon Tuff standards [28.48 ± 0.06 Ma; 32] were also analyzed (zFCT-61 and zFCT62 in table 1). For each sample, 3 single zircon aliquots were run with transparent euhedral grain radius higher than 70 μm, without inclusions and/or fractures. After measurement of their dimensions for $\alpha$-correction [33] and pictured, each grain was packed into a Nb foil envelope. $^{4}$He was then extracted from each pack in on in-house built He extraction line with successive 15-min-heatings under a focused beam of a 45 W diode laser (1250°C), until $^{4}$He yields were under 1% of total. After adding a known amount of purified $^{3}$He spike, $^{3}$He/$^{4}$He ratios were measured with a Pfiffer Vaccuum Prisma quadrupole mass-spectrometer. Typical errors are in range of 1.5-2% (1 $\sigma$). Samples were analyzed in groups of 36. In each group, 2 Fish Canyon Tuff (FTC) zircon standards were included to ensure accuracy, reproducibility, and reliability of the data. After He extraction, zircons were dissolved in high-pressure dissolution vessels with concentrated HF and $HNO_3$ at 200°C for 96 h. Prior dissolution, samples were spiked with mixed $^{235}$U, $^{230}$Th and $^{149}$Sm spike. Isotopic ratios are measured with iCAP Q ICP-MS. Additional blanks analyses controlled the analytical accuracy. The raw data were reduced using Helios software package (R. Kislitsyn and S. Stockli). To test different scenarios, we computed the $\alpha$-dose (D$\alpha$) for each zircon dated with ZHe methodology with the equation (1) presented in [34].

For ZFT dating at the GTC laboratory, zircon crystals were mounted in PFA Teflon® and polished [35]. Spontaneous fission-tracks were revealed by etching the grain mounts with a NaOH:KOH melt at 228°C in a covered Teflon dish heated by a laboratory oven for ~22-37 h. The samples were irradiated at the FRM II reactor (Garching, Germany). Fission tracks were counted dry at the GTC platform with an Olympus BH2 microscope at 1250x magnification. ZFT central ages were calculated with the RadialPlotter software [36],

using a ζ-value of 131.49 +/- 5.4 (M. Bernet) for the IRMM-541 uranium dosimeter glass (50 ppm U).

**Table 1.** Zircon (U-Th)/He data.

| Sample number | Age (Ma) | Err (Ma) | U[2] (ppm) | U[2] (ng) | Th[2] (ppm) | Th[2] (ng) | $^{147}$Sm[2] (ppm) | eU (ppm) | Th/U | He[2] (nmol/g) | Err. He (nmol/g) | Mass (µg) | Ft | ESR | Raw age (Ma) | Err. (Ma) |
|---|---|---|---|---|---|---|---|---|---|---|---|---|---|---|---|---|
| zFCT-61[1] | 30.7 | 2.3 | 373.0 | 2.3 | 191.9 | 1.2 | 0.0 | 417.1 | 0.5 | 53.0 | 4.2 | 6.1 | 0.8 | 49.8 | 23.5 | 1.7 |
| zFCT-62[1] | 29.8 | 2.2 | 315.3 | 1.9 | 168.2 | 1.0 | 0.0 | 354.0 | 0.5 | 44.0 | 3.5 | 6.2 | 0.8 | 51.5 | 23.0 | 1.7 |
| zAB1720-1 | 25.8 | 1.9 | 470.4 | 4.5 | 400.7 | 3.8 | 0.0 | 562.6 | 0.9 | 62.2 | 5.0 | 9.6 | 0.8 | 57.2 | 20.4 | 1.5 |
| zAB1720-2 | 1.5 | 0.1 | 403.1 | 4.8 | 32.3 | 0.4 | 0.0 | 410.5 | 0.1 | 2.8 | 0.2 | 11.9 | 0.8 | 62.5 | 1.3 | 0.1 |
| zAB1720-3 | 26.8 | 2.0 | 452.7 | 5.0 | 332.8 | 3.6 | 0.0 | 529.3 | 0.7 | 61.7 | 4.9 | 11.0 | 0.8 | 61.4 | 21.5 | 1.6 |
| zAB1764-1 | 2.1 | 0.2 | 516.0 | 6.9 | 248.1 | 3.3 | 0.0 | 573.1 | 0.5 | 5.4 | 0.4 | 13.3 | 0.8 | 65.5 | 1.7 | 0.1 |
| zAB1764-2 | 2.6 | 0.2 | 675.2 | 8.5 | 272.7 | 3.4 | 0.0 | 738.0 | 0.4 | 8.4 | 0.7 | 12.6 | 0.8 | 64.3 | 2.1 | 0.2 |
| zAB1764-3 | 2.4 | 0.2 | 440.2 | 6.1 | 152.5 | 2.1 | 0.1 | 475.4 | 0.3 | 5.1 | 0.4 | 13.8 | 0.8 | 66.7 | 2.0 | 0.1 |
| zAB1765-1 | 3.2 | 0.2 | 541.9 | 4.3 | 298.8 | 2.4 | 0.1 | 610.7 | 0.6 | 8.3 | 0.7 | 7.9 | 0.8 | 55.5 | 2.5 | 0.2 |
| zAB1765-2 | 2.1 | 0.2 | 597.0 | 4.7 | 149.2 | 1.2 | 0.0 | 631.3 | 0.2 | 5.5 | 0.4 | 7.9 | 0.8 | 55.7 | 1.6 | 0.1 |
| zAB1765-3 | 2.1 | 0.2 | 459.1 | 5.2 | 147.9 | 1.7 | 0.0 | 493.2 | 0.3 | 4.6 | 0.4 | 11.4 | 0.8 | 64.3 | 1.7 | 0.1 |
| zAB1766-1 | 4.0 | 0.3 | 503.9 | 3.3 | 312.4 | 2.0 | 0.0 | 575.9 | 0.6 | 9.6 | 0.8 | 6.5 | 0.8 | 51.3 | 3.1 | 0.2 |
| zAB1766-2 | 2.2 | 0.2 | 364.3 | 2.9 | 237.4 | 1.9 | 0.1 | 419.0 | 0.7 | 4.0 | 0.3 | 8.1 | 0.8 | 57.1 | 1.8 | 0.1 |
| zAB1766-3 | 1.9 | 0.1 | 403.0 | 3.1 | 141.0 | 1.1 | 0.0 | 435.5 | 0.3 | 3.6 | 0.3 | 7.6 | 0.8 | 54.0 | 1.5 | 0.1 |
| zAB1767-1 | 2.5 | 0.2 | 464.8 | 4.0 | 182.4 | 1.6 | 0.0 | 506.8 | 0.4 | 5.4 | 0.4 | 8.6 | 0.8 | 57.9 | 2.0 | 0.1 |
| zAB1767-2 | 3.3 | 0.2 | 313.7 | 2.4 | 115.9 | 0.9 | 0.0 | 340.4 | 0.4 | 4.7 | 0.4 | 7.8 | 0.8 | 55.8 | 2.6 | 0.2 |
| zAB1767-3 | 2.4 | 0.2 | 613.7 | 7.0 | 220.0 | 2.5 | 0.1 | 664.3 | 0.4 | 7.1 | 0.6 | 11.4 | 0.8 | 63.5 | 2.0 | 0.1 |
| zAB1768-1 | 2.3 | 0.2 | 1017.0 | 8.7 | 270.9 | 2.3 | 0.0 | 1079.4 | 0.3 | 10.5 | 0.8 | 8.6 | 0.8 | 58.5 | 1.8 | 0.1 |
| zAB1768-2 | 4.1 | 0.3 | 353.6 | 1.5 | 182.2 | 0.8 | 0.0 | 395.5 | 0.5 | 6.6 | 0.5 | 4.4 | 0.7 | 46.5 | 3.1 | 0.2 |
| zAB1768-3 | 3.3 | 0.2 | 1130.6 | 8.2 | 486.0 | 3.5 | 0.1 | 1242.6 | 0.4 | 17.3 | 1.4 | 7.2 | 0.8 | 55.4 | 2.6 | 0.2 |
| zAB1769-1 | 3.5 | 0.3 | 508.5 | 5.8 | 257.9 | 3.0 | 0.0 | 567.9 | 0.5 | 8.8 | 0.7 | 11.4 | 0.8 | 62.9 | 2.9 | 0.2 |
| zAB1769-2 | 3.3 | 0.2 | 538.3 | 7.3 | 247.1 | 3.4 | 0.1 | 595.2 | 0.5 | 8.6 | 0.7 | 13.6 | 0.8 | 66.0 | 2.7 | 0.2 |
| zAB1769-3 | 2.4 | 0.2 | 1176.3 | 9.3 | 489.7 | 3.9 | 0.0 | 1289.1 | 0.4 | 13.3 | 1.1 | 7.9 | 0.8 | 55.9 | 1.9 | 0.1 |

[1] Fish Canyon Tuff standards.

[2] Typical errors on U, Th, Sm and He measurements are in range of 1.5-2% (1σ). The reproducibility for zircons is based on ongoing measurements of standards and is at 7.3%.

## 4. Results

The six samples collected along the Inca trail (AB-12-64 to AB-17-69) analyzed with ZHe yield mean ages ranging from 2.4 ± 0.3 to 3.2 ± 0.9 Ma, giving a self-consistent age-elevation trend (Table 1: Figure 2). The aliquots of each sample are also consistent themselves. On the contrary, the lowest and 6-km-laterally-offset sample (AB-17-20) is less consistent: 1 aliquot is young (1.5 ± 0.1 Ma) and fit with the age-elevation trend whereas the two other aliquots present consistent old ages of ~25 Ma (Figure 2). In addition, the ZHe data do not show any age – effective uranium (eU) content or age – equivalent sphere radius (ESR) correlation (Figure 3).

The three new ZFT data range from 5.4 ± 0.3 Ma (AB-17-64) to 7.1 ± 0.4 (AB-17-68) (Table 2), are consistent with the other thermochronometers following the same age-elevation trend (Figure 2).

These new ZHe and ZFT data are much younger, and thus apparently incompatible with the two highest AFT data (AB-17-68 and AB-17-69 from [19]) in the profile. We thus revised the counting of these two AFT samples (Figure 2). In fact, both of the highest AFT samples are difficult to date because of poor apatite quality (fractures, inclusions) as mentioned in [19], these two samples yield unreliable AFT ages. After revision, the highest sample (AB-17-69) gives an AFT age more compatible with the zircon data ($3.1^{+3.2}_{-1.6}$ Ma), but still not reliable because of the few grains (10) dated, and because of the low apatite quality and U zonation. The second highest sample (AB-17-68) with a central age of $18.5^{+5.1}_{-4.0}$ Ma remains still older than other samples in the profile. Here also, the very low counts questions the validity of this age (Table 3). For these reasons, we will not base the following discussion on the highest fission-track data in the profile.

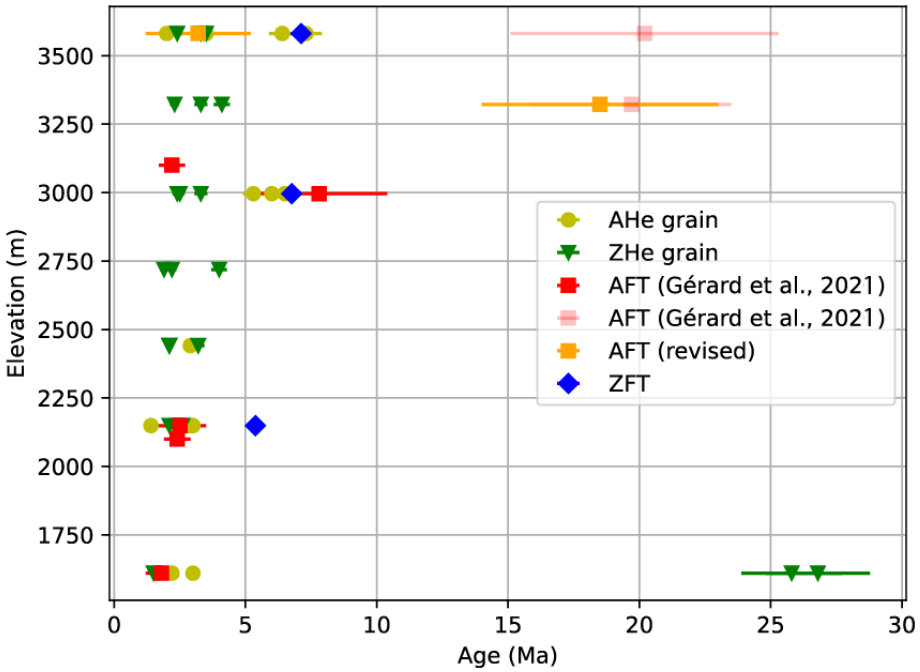


**Figure 2.** Ages-elevation of the Machu Picchu profile with AHe, ZHe, AFT and ZFT data [19; this study]. The two upper AFT data outside of the age-elevation trend were revised for this study.

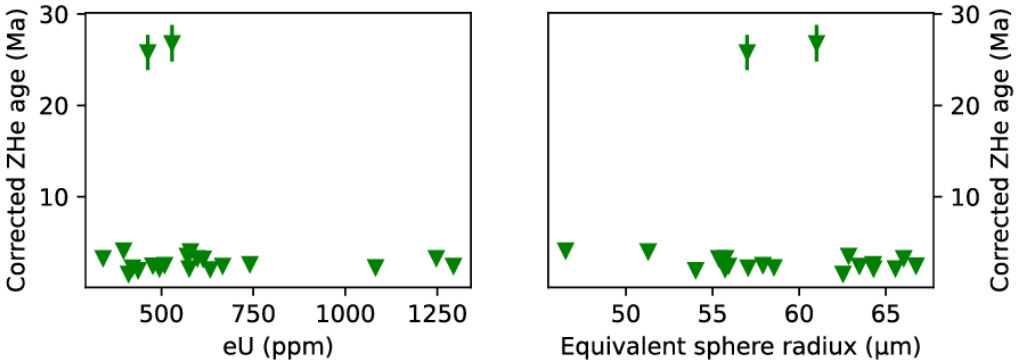


**Figure 3.** ZHe grain age of all the samples from the Machu Picchu vertical profile in function of the equivalent Uranium concentration (eU; left panel) and the equivalent sphere radius (ESR, right panel). Error bars are mostly smaller than the size of the points. There are no clear trends.

**Table 2.** Zircon fission track data[1].

| Sample | n | $\rho_s$ ($10^6$ cm$^{-2}$) | $N_s$ | $\rho_i$ ($10^6$ cm$^{-2}$) | $N_i$ | $\rho_d$ ($10^5$ cm$^{-2}$) | $P$ ($\chi^2$) | Dispersion (%) | Age (Ma) | ± 1$\sigma$ | U (ppm) | ± 2$\sigma$ |
|---|---|---|---|---|---|---|---|---|---|---|---|---|
| AB-17-64 | 20 | 1.4 | 587 | 6.7 | 2851 | 3.9 | 10.1 | 11.9 | 5.4 | 0.3 | 858 | 41 |
| AB-17-67 | 20 | 1.1 | 467 | 4.1 | 1776 | 3.9 | 59.2 | 0.7 | 6.8 | 0.4 | 528 | 29 |
| AB-17-68 | 20 | 1.2 | 418 | 4.4 | 1510 | 3.9 | 78.6 | 0.3 | 7.1 | 0.4 | 559 | 32 |

[1] Fission-track age is given as Central Age [37] calculated with the Radialplotter software [36]. Samples were counted dry with a BH2 Olympus microscope at 1250x magnification. Ages were calculated using a $\zeta$-value of 131.49 ± 5.4 for the IRMM 541 uranium dosimeter glass (50 ppm U). n: number of grains analyzed; ρs: spontaneous track density; Ns: number of spontaneous tracks; ρi: induced track density; Ni: number of induced track; ρd: dosimeter tracks density; P($\chi^2$): probability to obtain the $\chi^2$ value for n degrees of freedom (n = N° of crystals – 1).

**Table 3.** Revised apatite fission-track data for the Machu Picchu profile[1].

| Sample | n | $\rho_s$ ($10^5$ cm$^{-2}$) | $N_s$ | $\rho_i$ ($10^5$ cm$^{-2}$) | $N_i$ | $\rho_d$ ($10^5$ cm$^{-2}$) | $P$ ($\chi^2$) | Dispersion (%) | Central age (Ma) | ± 2$\sigma$ | U (ppm) | ± 1$\sigma$ | n Dpar[2] | MDpar ($\mu m$)[2] | n TL[2] | MTL ($\mu m$)[2] |
|---|---|---|---|---|---|---|---|---|---|---|---|---|---|---|---|---|
| AB-17-68 | 10 | 4.8 | 78 | 53.3 | 851 | 14.3 | 69.4 | 0.2 | 18.5 | 5.1 | 53 | 4 | 74 | 1.5 | N.D.[3] | N.D.[3] |
| AB-17-69 | 11 | 3.0 | 8 | 19.3 | 522 | 14.4 | 45.2 | 13.6 | 3.1 | 3.2 | 19 | 2 | 42 | 1.0 | 3 | 11.9 |

[1] Fission-track age is reported as central age [37]. Samples were counted dry with a BX51 Olympus microscope at 1250x magnification. Ages were calculated with the BINOMFIT program [38], using a $\zeta$-value of 270.90 ± 9.61 and the IRMM 540 uranium glass standard (15 ppm U). n: number of grains analyzed; ρs: spontaneous track density; Ns: number of spontaneous tracks; ρi: induced track density; Ni: number of induced track; ρd: dosimeter tracks density; P($\chi^2$): probability to obtain the $\chi^2$ value for n degrees of freedom (n = N° of crystals – 1); n Dpar: number of Dpar measured; MDpar: mean Dpar value, *i.e.* average etch pit diameter of fission-track; n TL: number of track lengths measured; MTL: mean track lengths of horizontally confined tracks.

[2] Reported from [19].

[3] No data.

## 5. Discussion

### *5.1. Revisiting the ZHe temperature sensitivity*

The new ZHe and ZFT age-elevation trends are consistent with the ones obtained with AHe and AFT data, and curiously, the ZHe data are younger or equivalent than usually lower closure temperature thermochronometers such as AHe and AFT (Figure 2). The ZFT data are consistent with previous data (AHe and AFT; Figure 2) and confirm previous geological interpretations [19,26]. Whereas all ZHe ages, at the exception of the lowest and more distant sample (AB-17-20), are younger than AFT and AHe dates from the same samples (Figure 2). This suggests that those samples present a ZHe closure temperature of ~80°C similar to the AHe system, which is lower than the classically expected [100-200°C; 1]. One can argue that an analytic issue occurred during the analysis. But the two Fish Canyon Tuff zircons standards analysis (zFCT-6x in table 1) give acceptable results (30.7 ± 2.3 Ma and 29.8 ± 2.2 Ma for a 28.48 ± 0.06 Ma age reference [32], ruling out any strong analytical bias.

Similar observations have been made by [14] who developed the ZRDAAM model, based on correlations between ZHe ages and effective uranium content. They proposed that low closure temperatures are due to middle-low (~$10^{16}$ $\alpha$/g with a Tc = ~120°C) or high annealing damages (>>$10^{18}$ $\alpha$/g). In order to test ZRDAAM model [14], we used HeFTy model [39] in forward mode in an attempt to reproduce AHe, AFT, ZHe and ZFT ages we obtained. We fed the model with a time-temperature history compatible with the one proposed by [19,26]. Modeling reveals that ZHe ages are younger than ZFT ages and close to AHe and AFT ages, but still older than AHe ages (Figure 4). The current ZHe model is thus not sufficiently accurate for very low $\alpha$-dose and cannot robustly explain the observations. [17] proposed a model similar to the ZRDAAM model in terms of Tc/$\alpha$-dose relationship independently of any age/eU or age/ESR correlation or any annealing damages effects. The latter model extends the $\alpha$-dose range to the low values and indirectly proposes a lower ZHe closure temperature than the ZRDAAM model for very low $\alpha$-dose, based on volcanic zircon data previously published [18].

In batholiths that cool rapidly, the $\alpha$-dose upper limit could be approximated by its crystallization age. But here, high $\alpha$-dose could not be geologically explained by the age of the sampled pluton. The granitic Machu Picchu Batholith emplaced at 222 ± 7 Ma [23]. The corresponding $\alpha$-dose computed for each dated zircon with this emplacement age is between 2.5×$10^{17}$ and ~1×$10^{18}$ $\alpha$/g if we assume that all produced alpha damage are preserved in the zircon crystals (Table 4). Following the trapping model [17], this value is still too low to allow for ZHe closure temperature to be lower than 80°C. However, it is interesting to note that the ZFT ages produced on the same samples present young ages <7 Ma, indicating that all fission-tracks produced since the crystallization have been annealed. The relatively low observed spontaneous track densities <1.4x$10^{6}$ tracks/cm$^2$ despite the relatively high U concentration (600-800 ppm) of the analyzed zircons indicates that accumulation of $\alpha$-radiation damage may not be significant (<4x$10^{16}$ $\alpha$/g) in the Machu Picchu batholith zircons (Table 2; Figure 5; [40]), because of relatively high temperatures (*i.e.* >300°C) before ~7 Ma. This interpretation is supported by the fact that the analyzed zircons were colorless. [41] had shown that color in zircon is related to the accumulation of $\alpha$-damage, but that color is lost when zircons are heated or reside at ambient temperatures of 325-475°C, with full color resetting, and therefore annealing of $\alpha$-damage, being possible at temperatures as low as 350°C [42]. Consequently, following the conclusions derived from the ZFT data, we can consider that the $\alpha$-damage produced since crystallization has been annealed and only started accumulating since about <7 Ma. In that case, the oldest ZFT age at ~7 Ma indicates that it should have begun to cool before this date. Cooling initiation at 7 Ma would induce a $\alpha$-dose of about 0.6×$10^{15}$ to 4×$10^{16}$ $\alpha$/g (Figure 6). Consequently, we propose that at very low damage dose, the ZHe closure temperature to be close to 80°C (Figure 7). This result agrees with the prediction from [17] using theoretical approach of the diffusion behavior in zircon (Figure 7). This result has major implication

because it demonstrates that the ZHe method has a large range of temperature sensitivity. A low closure temperature, similar to AHe should be considered for zircons having a low damage dose (Figure 7).

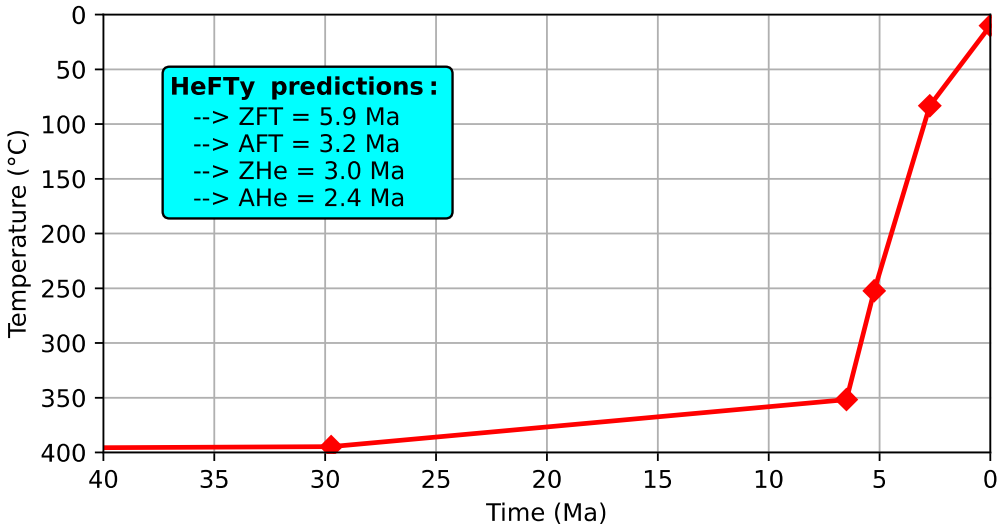


**Figure 4.** Time-temperature path used in HeFTy [39] to predict AHe, ZHe, AFT and ZFT ages (in the blue box) using respectively the models and models parameters of RDAMM [12], ZRDAAM [14], [43] and [44]. This time-temperature path is an adaptation for higher closure temperature systems of the time temperature paths proposed for the southern Abancay Deflection by [26].

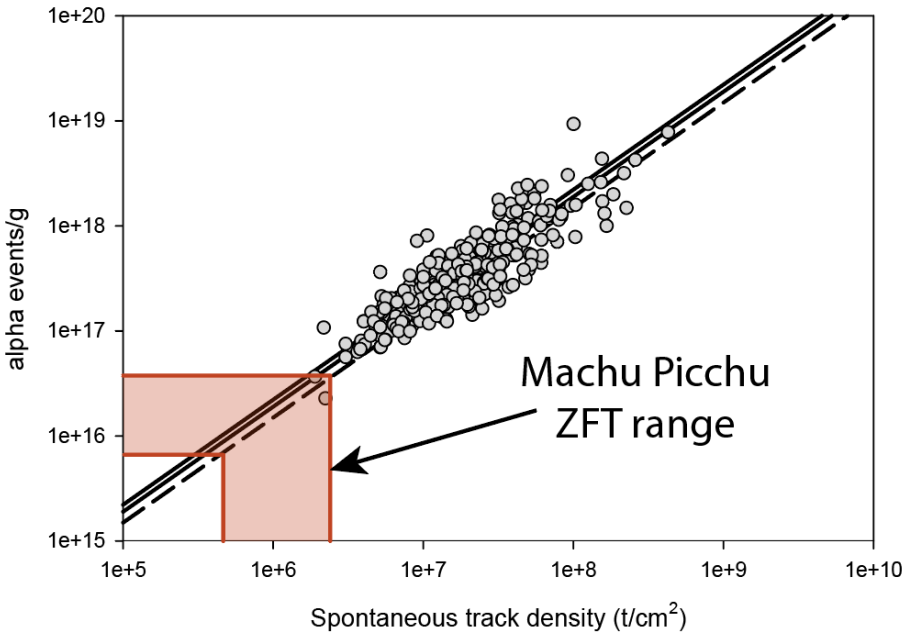


**Figure 5.** Plot of the Machu Picchu ZFT data (light red area) in the simplified Spontaneous track density ($\rho$s) and $\alpha$-dose relationship from [40]. Grey dots are the 336 zircons they analyzed, and the dashed and full lines represent respectively the approximate and full relationships they computed. Spontaneous tracks densities from the Machu Picchu's zircons indicate a $\alpha$-dose below $4\times10^{16}$ $\alpha$/g.

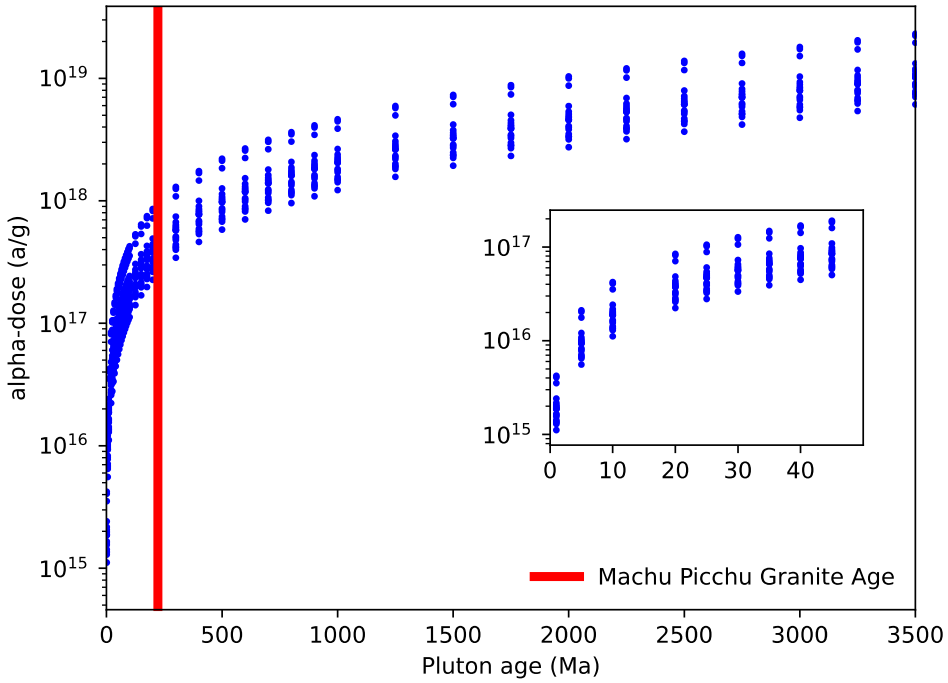


**Figure 6.** $\alpha$-dose in function of the age of a pluton computed for the samples of the Machu Picchu vertical profile (blue dots). The red vertical thick line corresponds to the ages of the Machu Picchu batholith [~222 Ma, 23]. Light red horizontal bands show the $\alpha$-dose values that are compatible with the ZHe data from the Machu Picchu. We estimated them with the relationship between the ZHe closure temperature, the alpha dose, and the estimated ZHe closure temperature from the Machu Picchu. The inset is a zoom for the first part of the graph.

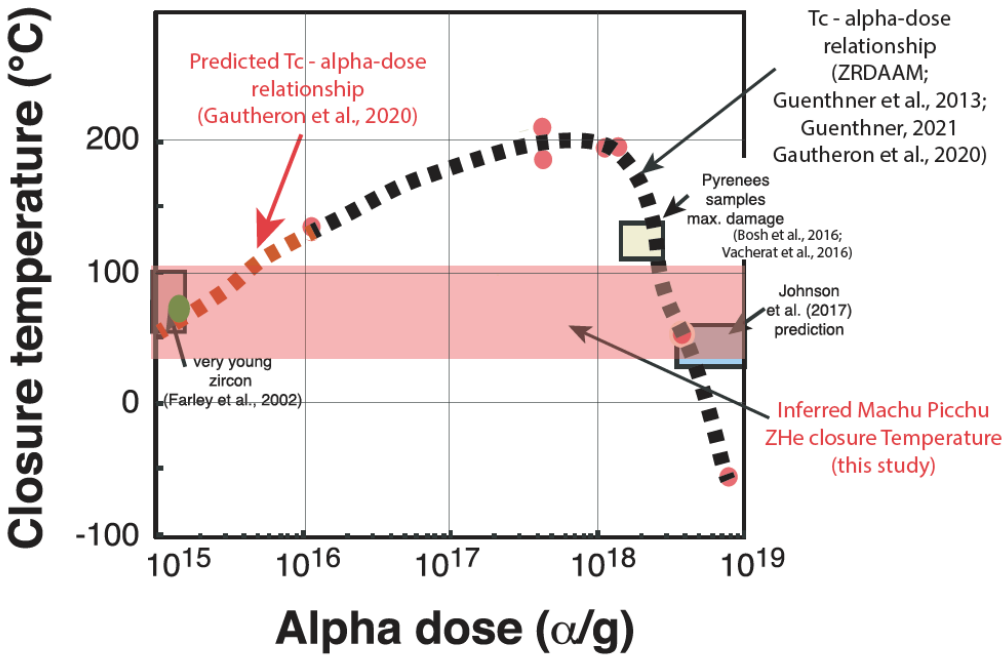


**Figure 7.** Update of the co-evolution of the closure temperature and the $\alpha$-dose (Fig. 10B of [17]) with our new data from the Machu Picchu profile (green dot). Red circles correspond to [14] data recalculated with the Density Functional Theory results (see details in [17]), the yellow box places Pyrenean samples [45,46] and the blue box represents [9] high

damaged zircons. The black dashed line shows the shape of the closure-temperature / $\alpha$-dose relationship presented in previous models. We add an estimation of the closure-temperature / $\alpha$-dose relationship inferred from [17] (red dashed line), and the estimated closure temperature of the ZHe from the Machu Picchu (this study, light red horizontal band).

**Table 4.** Closure temperature (Tc) estimation with a scenario implying a reheating between 5 and 8 Ma (case 1) and a simple scenario where the $\alpha$-dose received is only due because of the age of the Permo-Triasic pluton [222 Ma; 23], (case 2) or of a >1 Ga pluton (case 3). Tc is estimated for each aliquot by reporting computed $\alpha$-dose for each case on Figure 7.

| | Case 1: 5-8 Ma cooling | | | Case 2: Permo-Triasic pluton emplacement (222 Ma) without re-heating | | | Case 3: 1 Ga pluton emplacement without re-heating | | |
|---|---|---|---|---|---|---|---|---|---|
| **Sample number** | **Time ($10^6$ yr)** | **$\alpha$ -dose ($\alpha$/g)** | **Estimated Tc range (°C)[1]** | **Time ($10^6$ yr)** | **$\alpha$ -dose ($\alpha$/g)** | **Estimated Tc range (°C)[1]** | **Time ($10^9$ yr)** | **$\alpha$ -dose ($\alpha$/g)** | **Estimated Tc range (°C)[1]** |
| zAB1720-2 | 5 | $6.7.10^{15}$ | 40-60 | 222 | $3.0.10^{17}$ | 150-200 | 1 | $1.5.10^{18}$ | 110-130 |
| zAB1764-1 | 5 | $9.4.10^{15}$ | 50-90 | 222 | $4.2.10^{17}$ | 150-200 | 1 | $2.1.10^{18}$ | 100-120 |
| zAB1764-2 | 5 | $1.2.10^{16}$ | 100-140 | 222 | $5.5.10^{17}$ | 150-200 | 1 | $2.7.10^{18}$ | 100-120 |
| zAB1764-3 | 5 | $7.8.10^{15}$ | 50-90 | 222 | $3.5.10^{17}$ | 150-200 | 1 | $1.7.10^{18}$ | 100-130 |
| zAB1765-1 | 5 | $1.0.10^{16}$ | 50-90 | 222 | $4.5.10^{17}$ | 150-200 | 1 | $2.2.10^{18}$ | 100-120 |
| zAB1765-2 | 5 | $1.0.10^{16}$ | 100-140 | 222 | $4.7.10^{17}$ | 150-200 | 1 | $2.3.10^{18}$ | 100-120 |
| zAB1765-3 | 5 | $8.1.10^{15}$ | 50-90 | 222 | $3.7.10^{17}$ | 150-200 | 1 | $1.8.10^{18}$ | 100-130 |
| zAB1766-1 | 5 | $9.4.10^{15}$ | 50-90 | 222 | $4.3.10^{17}$ | 150-200 | 1 | $2.1.10^{18}$ | 100-120 |
| zAB1766-2 | 5 | $6.9.10^{15}$ | 50-90 | 222 | $3.1.10^{17}$ | 150-200 | 1 | $1.5.10^{18}$ | 100-130 |
| zAB1766-3 | 5 | $7.1.10^{15}$ | 50-90 | 222 | $3.2.10^{17}$ | 150-200 | 1 | $1.6.10^{18}$ | 100-130 |
| zAB1767-1 | 6 | $9.9.10^{15}$ | 50-90 | 222 | $3.8.10^{17}$ | 150-200 | 1 | $1.8.10^{18}$ | 100-130 |
| zAB1767-2 | 6 | $6.7.10^{15}$ | 50-90 | 222 | $2.5.10^{17}$ | 150-200 | 1 | $1.2.10^{18}$ | 120-190 |
| zAB1767-3 | 6 | $1.3.10^{16}$ | 100-140 | 222 | $4.9.10^{17}$ | 150-200 | 1 | $2.4.10^{18}$ | 100-120 |
| zAB1768-1 | 7 | $2.5.10^{16}$ | 50-90 | 222 | $8.0.10^{17}$ | 150-200 | 1 | $3.9.10^{18}$ | 30-60 |
| zAB1768-2 | 7 | $9.1.10^{15}$ | 50-90 | 222 | $2.9.10^{17}$ | 150-200 | 1 | $1.4.10^{18}$ | 100-130 |
| zAB1768-3 | 7 | $2.8.10^{16}$ | 100-140 | 222 | $9.2.10^{17}$ | 150-200 | 1 | $4.5.10^{18}$ | 30-60 |
| zAB1769-1 | 8 | $1.5.10^{16}$ | 100-140 | 222 | $4.2.10^{17}$ | 150-200 | 1 | $2.0.10^{18}$ | 100-120 |
| zAB1769-2 | 8 | $1.6.10^{16}$ | 100-140 | 222 | $4.4.10^{17}$ | 150-200 | 1 | $2.1.10^{18}$ | 100-120 |
| zAB1769-3 | 8 | $3.4.10^{16}$ | 100-140 | 222 | $9.5.10^{17}$ | 150-200 | 1 | $4.6.10^{18}$ | 30-60 |

[1] Tc estimated from figure 10b in [17], using $\alpha$ -dose values.

5.2. Geological implication

In a relatively old batholith as the Machu Picchu Batholith, two geological processes could explain a low $\alpha$-dose: 1) an important reheating >300°C that reset all $\alpha$-dose before 7 Ma will induce such low $\alpha$-dose, or 2) the batholith stayed at a relatively important temperature until recently, preventing any radiation damage effects until this date. Interestingly, previous studies [19,26], did not find evidence of any recent important reheating. Moreover, our ZFT data are not reset and show a low amount of tracks. [47] demonstrated that annealing of ZFT is much more temperature and time sensitive than healing of radiation damages in zircons. In our setting, zircon samples accumulated very few radiation damages in their lattice before minimal 7 Ma, suggesting that no important reheating occurred recently. The simplest explanation, close to the time-temperature path used in figure 4, is that the batholith stayed at a temperature higher than ~300°C until recently (before 7 Ma, oldest age of our dataset), before cooling below that temperature. AHe and AFT data in the southern part of the Abancay Deflection indicate a cooling acceleration at 5 ± 2 Ma from 100-150°C [26]. Our ZHe and ZFT data show that this cooling acceleration may have initiated at least sometimes before 7 Ma and from a higher temperature (300°C) than previously proposed. It suggests thus a more important cooling rate (>43°C/Myr) than the one deduced from AHe and AFT data (21±6°C/Myr) [19]. AHe and AFT derived exhumation rate ranges between 0.6 and 1.9 km/Myr [19]. Taking into account ZFT data, it leads to an exhumation rate within the range of 1.3 and 3.0 km/Myr since ~7 Ma, assuming end-members values for geothermal gradient of 26 ± 8°C/km [48] or 18 ± 4°C/km [26]. Our new data complete and strengthen the previous interpretations in terms of exhumation rates and further validate the tectonic syntaxis implication for the Abancay Deflection as proposed in [26].

## 6. Conclusions

We provide new zircon fission track and zircon (U-Th)/He data to the Machu Picchu (Abancay Deflection, Peru) age–elevation profile. The new zircon ages are young (< 7 Ma), reinforcing our previous young exhumation pulse (~5 Ma) and further favor the interpretation of the Abancay Deflection as a tectonic syntaxis.

The ZHe system evidences closure temperature lower than for apatite fission-track and apatite (U-Th)/He systems. This apparent contradiction, explained by low radiation damages in the zircons, is rather due to a simple time-temperature history with a long stay at elevated temperature before cooling than to the age of the Machu Picchu batholith itself. In the present geological setting, these new data 1) evidence that ZHe system is a thermochronometer not only sensible to temperatures higher than 150°C, but, in some cases, to temperature lower than 100-110°C or even 80°C, and 2) complete a setting (young ZHe ages, very low $\alpha$-dose) that was predicted, but not observed, by recent modeling. Our work highlights the importance to be aware of both the $\alpha$-dose and the time since when damages accumulate to avoid biases when interpreting thermochronological data. In summary, our ZHe data open a door to further experiment and better understand He behavior in low radiation damaged zircons.

**Supplementary Materials:** The following are available online at www.mdpi.com/xxx/s1, Figure S1: binomfit output file for sample AB-17-68 (AFT dating), Figure S2: binomfit output file for sample AB-17-69 (AFT dating), Figure S3: binomfit output file for sample AB-17-64 (ZFT dating), Figure S4: binomfit output file for sample AB-17-67 (ZFT dating), Figure S5: binomfit output file for sample AB-17-68 (ZFT dating).

**Author Contributions:** Conceptualization: X.R., C.G. and L.A.; methodology: C.G., M.B., M.Ba., D.G. and B.G.; software: X.R., M.B. and M.Ba.; validation: B.G., X.R. and C.G.; investigation: B.G., X.R., L.A., M. B., C.G. and D.G.; writing—original draft preparation: X.R.; writing—review and editing: X.R., B.G., C.G., D.G., L.A. and M.B.; visualization: X.R., C.G., M.B. and B.G.; B.G., All authors have read and agreed to the published version of the manuscript.

**Funding:** This work was funded by the Agence Nationale de la Recherche (12-NS06-0005-01 for He analyses), Institut de Recherche pour le Développement, l'Institut des Sciences de la Terre and Institut national des Sciences de l'Univers (INSU – CNRS).



**Acknowledgments:** We thank SERNANP, INGEMMET (Cuzco-PATA convenio 006-2016-Fondecyt), and F. Astete (National Archaeological Park of Machu Picchu) for permission to work along the Inca trail and for provided facilities. We thank F. Delgado and C. Benavente for field assistance, and P.H. Leloup, G. Mahéo (Géode laboratory, Lyon) and the GTC platform (F. Coeur and F. Sénebier, ISTerre, Grenoble) for sample processing, as well as R. Pinna-Jamme and F. Haurine for assistance during AFT, ZFT and AHe dating.

**Conflicts of Interest:** The authors declare no conflict of interest.

## References

1. Ault, A.K.; Gautheron, C.; King, G.E. Innovations in (U–Th)/He, Fission Track, and Trapped Charge Thermochronometry with Applications to Earthquakes, Weathering, Surface-Mantle Connections, and the Growth and Decay of Mountains. *Tectonics* **2019**, *38*, 3705–3739, doi:10.1029/2018TC005312.

2. Reiners, P.W.; Brandon, M.T. Using Thermochronology to Understand Orogenic Erosion. *Annual Review of Earth and Planetary Sciences* **2006**, *34*, 419–466, doi:10.1146/annurev.earth.34.031405.125202.

3. Reiners, P.W.; Farley, K.A.; Hickes, H.J. He Diffusion and (U–Th)/He Thermochronometry of Zircon: Initial Results from Fish Canyon Tuff and Gold Butte. *Tectonophysics* **2002**, *349*, 297--308, doi:10.1016/S0040-1951(02)00058-6.

4. Reiners, P.W.; Spell, T.L.; Nicolescu, S.; Zanetti, K.A. Zircon (U-Th)/He Thermochronometry: He Diffusion and Comparisons with $^{40}Ar/^{39}Ar$ Dating. *Geochim. Cosmochim. Acta* **2004**, *68*, 1857–1887.

5. Reiners, P.W. Zircon (U-Th)/He Thermochronometry. *Reviews in Mineralogy & Geochemistry* **2005**, *58*, 151–179.

6. Bernet, M. A Field-Based Estimate of the Zircon Fission-Track Closure Temperature. *Chemical Geology* **2009**, *259*, 181–189.

7. Brandon, M.T.; Roden-Tice, M.K.; Garver, J.I. Late Cenozoic Exhumation of the Cascadia Accretionary Wedge in the Olympic Mountains, Northwest Washington State. *Geol Soc Am Bull* **1998**, *110*, 985–1009.

8. Guenthner, W.R.; Reiners, P.W.; Tian, Y. Interpreting Date--EU Correlations in Zircon (U-Th)/He Datasets: A Case Study from the Longmen Shan, China. *Earth and Planetary Science Letters* **2014**, *403*, 328–339, doi:http://dx.doi.org/10.1016/j.epsl.2014.06.050.

9. Johnson, J.E.; Flowers, R.M.; Baird, G.B.; Mahan, K.H. "Inverted"Zircon and Apatite (U--Th)/He Dates from the Front Range, Colorado: High-Damage Zircon as a Low-Temperature (<50 °C) Thermochronometer. *Earth and Planetary Science Letters* **2017**, *466*, 80–90, doi:http://dx.doi.org/10.1016/j.epsl.2017.03.002.

10. Shuster, D.L.; Flowers, R.M.; Farley, K.A. The Influence of Natural Radiation Damage on Helium Diffusion Kinetics in Apatite. *Earth and Planetary Science Letters* **2006**, *249*, 148--161, doi:10.1016/j.epsl.2006.07.028.

11. Flowers, R.M.; Shuster, D.L.; Wernicke, B.P.; Farley, K.A. Radiation Damage Control on Apatite (U-Th)/He Dates from the Grand Canyon Region, Colorado Plateau. *Geology* **2007**, *35*, 447–450.

12. Flowers, R.M.; Ketcham, R.A.; Shuster, D.L.; Farley, K.A. Apatite (U-Th)/He Thermochronometry Using a Radiation Damage Accumulation and Annealing Model. *Geochimica et Cosmochimica Acta* **2009**, *73*, 2347–2365.

13. Gautheron, C.; Tassan-Got, L.; Barbarand, J.; Pagel, M. Effect of Alpha-Damage Annealing on Apatite (U–Th)/He Thermochronology. *Chemical Geology* **2009**, *266*, 157–170, doi:https://doi.org/10.1016/j.chemgeo.2009.06.001.

14. Guenthner, W.R.; Reiners, P.W.; Ketcham, R.A.; Nasdala, L.; Giester, G. Helium Diffusion in Natural Zircon: Radiation Damage, Anisotropy, and the Interpretation of Zircon (U-Th)/He Thermochronology. *American Journal of Science* **2013**, *313*, 145, doi:10.2475/03.2013.01.

15. Guenthner, W.R. Implementation of an Alpha Damage Annealing Model for Zircon (U-Th)/He Thermochronology With Comparison to a Zircon Fission Track Annealing Model. *Geochemistry, Geophysics, Geosystems* **2021**, *22*, e2019GC008757, doi:10.1029/2019GC008757.

16. Ternois, S.; Odlum, M.; Ford, M.; Pik, R.; Stockli, D.; Tibari, B.; Vacherat, A.; Bernard, V. Thermochronological Evidence of Early Orogenesis, Eastern Pyrenees, France. *Tectonics* **2019**, *38*, 1308--1336, doi:10.1029/2018TC005254.

17. Gautheron, C.; Djimbi, D.M.; Roques, J.; Balout, H.; Ketcham, R.A.; Simoni, E.; Pik, R.; Seydoux-Guillaume, A.-M.; Tassan-Got, L. A Multi-Method, Multi-Scale Theoretical Study of He and Ne Diffusion in Zircon. *Geochimica et Cosmochimica Acta* **2020**, 348--367.

18. Farley, K.A.; Kohn, B.P.; Pillans, B. The Effects of Secular Disequilibrium on (U–Th)/He Systematics and Dating of Quaternary Volcanic Zircon and Apatite. *Earth and Planetary Science Letters* **2002**, *201*, 117--125, doi:10.1016/S0012-821X(02)00659-3.

19. Gérard, B.; Audin, L.; Robert, X.; Gautheron, C.; van der Beek, P.; Bernet, M.; Benavente, C.; Delgado, F. Pliocene River Capture and Incision of the Northern Altiplano: Machu Picchu, Peru. *Journal of the Geological Society* **2021**, *178*, jgs2020-100, doi:10.1144/jgs2020-100.

20. Marocco, R. Etude géologique de la chaîne andine au niveau de la déflexion d'Abancay (Pérou). *Cahiers ORSTOM.Série Géologie* **1971**, *3*, 45–57.

21. Roperch, P.; Carlotto, V.; Ruffet, G.; Fornari, M. Tectonic Rotations and Transcurrent Deformation South of the Abancay Deflection in the Andes of Southern Peru. *Tectonics* **2011**, *30*, doi:10.1029/2010TC002725.

22. Mišković, A.; Spikings, R.A.; Chew, D.M.; Košler, J.; Ulianov, A.; Schaltegger, U. Tectonomagmatic Evolution of Western Amazonia: Geochemical Characterization and Zircon U-Pb Geochronologic Constraints from the Peruvian Eastern Cordilleran Granitoids. *GSA Bulletin* **2009**, *121*, 1298–1324, doi:10.1130/B26488.1.

23. Carlier, G.; Grandin, G.; Laubacher, G.; Marocco, R.; Mégard, F. Present Knowledge of the Magmatic Evolution of the Eastern Cordillera of Peru. *Earth-Science Reviews* **1982**, *18*, 253--283, doi:10.1016/0012-8252(82)90040-X.

24. Perez, N.D.; Horton, B.K.; Carlotto, V. Structural Inheritance and Selective Reactivation in the Central Andes: Cenozoic Deformation Guided by Pre-Andean Structures in Southern Peru. *Tectonophysics* **2016**, *671*, 264–280, doi:http://dx.doi.org/10.1016/j.tecto.2015.12.031.

25. Kennan, L. Fission Track Ages and Sedimentary Provenance Studies in Peru, and Their Implications for Andean Paleogeographic Evolution, Stratigraphy and Hydrocarbon Systems. *VI INGEPET* **2008**, *13*, 17.

26. Gérard, B.; Robert, X.; Audin, L.; Valla, P.G.; Bernet, M.; Gautheron, C. Differential Exhumation of the Eastern Cordillera in the Central Andes: Evidence for South-Verging Backthrusting (Abancay Deflection, Peru). *Tectonics* **2021**, *40*, e2020TC006314, doi:10.1029/2020TC006314.

27. Carlier, G.; Lorand, J.P.; Liéárdenas, J. Potassic-Ultrapotassic Mafic Rocks Delineate Two Lithospheric Mantle Blocks beneath the Southern Peruvian Altiplano. *Geology* **2005**, *33*, 601–604, doi:10.1130/G21643.1.

28. Mamani, M.; Wörner, G.; Sempere, T. Geochemical Variations in Igneous Rocks of the Central Andean Orocline (13 °S to 18 °S): Tracing Crustal Thickening and Magma Generation through Time and Space. *Geological Society of America Bulletin* **2010**, *122*, 162–182.

29. Carlier, G.; Lorand, J.-P.; Bonhomme, M.; Carlotto, V. A Reappraisal of the Cenozoic Inner Arc Magmatism in Southern Peru: Consequences for the Evolution of the Central Andes for the Past 50 Ma.; 1996; pp. 551--554.

30. Ruiz, G.M.H.; Carlotto, V.; van Heiningen, P.V.; Andriessen, P.A.M. Steady-State Exhumation Pattern in the Central Andes - SE Peru. In Proceedings of the Thermochronological Methods: From Paleotemperature Constraints to Landscape evolution Models; Lisker, F., Ventura, B., Glasmacher, U.A., Eds.; Geological Society, London, Special Publications, 2009; Vol. 307, pp. 307–316.

31. Landry, K.R.; Coutand, I.; Whipp, D.M.; Grujic, D.; Hourigan, J.K. Late Neogene Tectonically Driven Crustal Exhumation of the Sikkim Himalaya: Insights from Inversion of Multithermochronologic Data. *Tectonics* **2016**, 2015TC004102, doi:10.1002/2015TC004102.

32. Schmitz, M.D.; Bowring, S.A. U-Pb Zircon and Titanite Systematics of the Fish Canyon Tuff: An Assessment of High-Precision U-Pb Geochronology and Its Application to Young Volcanic Rocks. *Geochimica et Cosmochimica Acta* **2001**, *65*, 2571--2587, doi:10.1016/S0016-7037(01)00616-0.

33. Farley, K.A.; Wolf, R.; Silver, L. The Effect of Long Alpha-Stopping Distances on (U-Th)/He Dates. *Geochimica et Cosmochimica Acta* **1996**, *60*, 4223–4229.

34. Nasdala, L.; Hanchar, J.M.; Kronz, A.; Whitehouse, M.J. Long-Term Stability of Alpha Particle Damage in Natural Zircon. *Chemical Geology* **2005**, *220*, 83--103, doi:10.1016/j.chemgeo.2005.03.012.

35. Bernet, M.; Garver, J.I. Fission-Track Analysis of Detrital Zircon. *Reviews in Mineralogy and Geochemistry* **2005**, *58*, 205--237, doi:10.2138/rmg.2005.58.8.

36. Vermeesch, P. RadialPlotter: A Java Application for Fission Track, Luminescence and Other Radial Plots. *Radiation Measurements* **2009**, *44*, 409--410, doi:10.1016/j.radmeas.2009.05.003.

37. Galbraith, R.F.; Laslett, G.M. Statistical Models for Mixed Fission Track Ages. *Nuclear Tracks and Radiation Measurements* **1993**, *21*, 459--470, doi:10.1016/1359-0189(93)90185-C.

38. Ehlers, T.A.; Chaudhri, T.; Kumar, S.; Fuller, C.W.; Willett, S.D.; Ketcham, R.A.; Brandon, M.T.; Belton, D.X.; Kohn, B.P.; Gleadow, A.J.W.; et al. Computational Tools for Low-Temperature Thermochronometer Interpretation. *Reviews in Mineralogy and Geochemistry* **2005**, *58*, 589--622, doi:10.2138/rmg.2005.58.22.

39. Ketcham, R.A. Forward and Inverse Modelling of Low-Temperature Thermochronology Data. *Rev. Mineral. Geoch.* **2005**, *84*, 1235–1255.

40. Bernet, M.; Brandon, M.T.; Garver, J.I.; Molitor, B.R. Fundamentals of Detrital Zircon Fission-Track Analysis for Provenance and Exhumation Studies with Examples from the European Alps. In *Detrital thermochronology - Provenance analysis, exhumation, and landscape evolution of mountain belts*; Bernet, M., Spiegel, C., Eds.; Geological Society of America, 2004; Vol. 378, p. 0 ISBN 978-0-8137-2378-5.

41. Garver, J.I.; Kamp, P.J.J. Integration of Zircon Color and Zircon Fission-Track Zonation Patterns in Orogenic Belts: Application to the Southern Alps, New Zealand. *Tectonophysics* **2002**, *349*, 203--219, doi:10.1016/S0040-1951(02)00054-9.

42. Gordon Gastil, R.; DeLisle, M.; Morgan, J. Some Effects of Progressive Metamorphism on Zircons. *GSA Bulletin* **1967**, *78*, 879--906, doi:10.1130/0016-7606(1967)78$[$879:SEOPMO$]$2.0.CO;2.

43. Ketcham, R.A.; Carter, A.; Donelick, R.A.; Barbarand, J.; Hurford, A. Improved Measurement of Fission-Track Annealing in Apatite Using c-Axis Projection. *American Mineralogist* **2007**, *92*, 789–798.

44. Yamada, R.; Murakami, M.; Tagami, T. Statistical Modelling of Annealing Kinetics of Fission Tracks in Zircon; Reassessment of Laboratory Experiments. *Chemical Geology* **2007**, *236*, 75--91, doi:10.1016/j.chemgeo.2006.09.002.

45. Bosch, G.; Teixell, A.; Jolivet, M.; Labaume, P.; Stockli, D.; Domènech, M.; Monié, P. Timing of Eocene--Miocene Thrust Activity in the Western Axial Zone and Chaînons Béarnais (West-Central Pyrenees) Revealed by Multi-Method Thermochronology. *From rifting to mountain building: the Pyrenean Belt* **2016**, *348*, 246--256, doi:10.1016/j.crte.2016.01.001.

46. Vacherat, A.; Mouthereau, F.; Pik, R.; Bellahsen, N.; Gautheron, C.; Bernet, M.; Daudet, M.; Balansa, J.; Tibari, B.; Pinna Jamme, R.; et al. Rift-to-Collision Transition Recorded by Tectono-Thermal Evolution of the Northern Pyrenees. *Tectonics* **2016**, 2015TC004016, doi:10.1002/2015TC004016.

47. Ginster, U.; Reiners, P.W.; Nasdala, L.; Chanmuang N., C. Annealing Kinetics of Radiation Damage in Zircon. *Geochimica et Cosmochimica Acta* **2019**, *249*, 225--246, doi:10.1016/j.gca.2019.01.033.

48. Barnes, J.B.; Ehlers, T.A.; McQuarrie, N.; O'Sullivan, P.B.; Tawackoli, S. Thermochronometer Record of Central Andean Plateau Growth, Bolivia (19.5∞S). *Tectonics* **2008**, *27*.